JUICE/GALA-J (2): Science targets of the GAnymede Laser Altimeter (GALA) for the JUICE mission

*Jun Kimura[1], Shunichi Kamata[2], Koji Matsumoto[3], Shoko Oshigami[8], Noriyuki Namiki[3], Kiyoshi Kuramoto[2], Sho Sasaki[1], Keigo Enya[4], Masanori Kobayashi[5], Shingo Kobayashi[6], Hiroshi Araki[3], Hirotomo Noda[3], Ko Ishibashi[5], Yoshifumi Saito[4], Hauke Hussmann[7], Kay Lingenauber[7]

1. Osaka University, 2. Hokkaido University, 3. National Astronomical Observatory Japan, 4. Institute of Space and Astronautical Science, 5. Chiba Insitute of Technology, 6. National Institute of Radiological Sciences, 7. Deutsches Zentrum für Luft- und Raumfahrt, 8. Kogakuin University

The JUpiter Icy Moons Explorer (JUICE), led by European Space Agency, has started development toward launch in 2022 (arrival at Jupiter in 2029, and Ganymede orbit insertion in 2032), and we are now developing the GALA instrument onboard JUICE spacecraft collaborating with German Aerospace Center (DLR) and other institutions in Europe. GALA will acquire the key information for understanding the evolution of Jovian icy moons and to play an essential role in the JUICE's purpose: exploration of deep habitat.

Jovian icy moon Ganymede, which is the largest moon in the Solar System and the primary target of the JUICE, can be said to be one of the typical solid bodies along with terrestrial planets in terms of its size and the intrinsic magnetic field originated from the metallic core. However, current knowledge provided by previous explorations is extremely limited since it comes from only several fly-bys. The JUICE will unveil the whole picture of Ganymede by the first orbiting in the history around extra-terrestrial moon. Expected new big picture of the origin and evolution of Ganymede will not only be a key to unveil the origin of diversity among the Solar System bodies, but also contribute to an understanding of exoplanets with a wide diversity.

The GALA will measure a distance between the spacecraft and the surface of icy moons and acquire the topography data (globally for Ganymede, and fly-by region for Europa and Callisto). It will be a first-ever laser altimetry for the icy object. Such information makes surface geologies clear and tremendously improves our understanding of the icy tectonics. By comparing their tectonic styles on the rocky planets/moons, GALA data leads to reconsider the Earth's plate tectonics. In addition, the GALA will confirm a presence/absence of the subsurface ocean by measuring tidal and rotational response, and the gravitational information reflecting the interior structure will be greatly improved. Furthermore, strength and waveform of reflected laser pulse have an information about surface reflectance at the laser wavelength and small-scale roughness. Finally we can see degrees of erosion and space weathering without being affected by illumination condition through GALA measurements.

In order to interpret and understand such measurements, accumulated studies for the Earth over the years will be effectively utilized: e.g., the data for surface topography, roughness and albedo will lead to describe the icy tectonics through the knowledge from terrestrial glaciology and experiments on impact and deformation process. The tidal measurements by GALA will also be a window to see its interior based on our knowledge and experiences cultivated through the past geodetic observations, e.g., the SELENE mission for the terrestrial Moon.

Characterization of the icy moons will be achieved not only from the GALA measurements but also synergy of other scientific instruments onboard JUICE spacecraft, for examples, surface images taken by optical camera (JANUS) will confirm the position of GALA laser footprint to complement the GALA "point" data for precise topographic mapping. A radar sounder (RIME) and a radio science experiment (3GM) probe the interior structure, especially interior of the icy crust to figure out an occurrence of tectonic features. A visible and infrared imaging spectrometer (MAJIS), an ultraviolet imaging spectrograph (UVS) and a

sub-millimeter wave instrument (SWI) will acquire a surface and atmosphere compositional data. A magnetometer (J-MAG) monitors moons' inductive response to the Jovian magnetic field and probes the subsurface ocean with the help of a particle environment package (PEP) and a radio and plasma wave investigation (RPWI). The GALA works closely together with these instruments and plays a leading and a supporting role to clarify the whole picture of Ganymede and other icy moons.

Period characteristics of Mercury's external magnetic field from MESSENGER magnetometer observation

*Takaaki Katsura[1], Hiroaki TOH[2]

1. Solar-Planetary Electromagnetism Laboratory, Department of Geophysics, Graduate School of Science, Kyoto University, 2. Data Analysis Center for Geomagnetism and Space Magnetism Graduate School of Science, Kyoto University

MESSENGER(MErcury Surface, Space Environment, Geochemistry, and Randing) is the first probe launched into Mercury centric orbit and has been observed electromagnetic circumstances including magnetic field over about four years since 2011.From this data the average shape and location of Mercury’s magnetopause and bow shock have determined (Winslow et al., 2013).Furthermore, from the studies of magnetic fields induced at the top of Mercury’s core by time-varying magnetospheric fields, the radius of Mercury’s core is determined (Johnson et al., 2016).

At present, however for the period of external magnetic variations, annual variation due to Mercury’s high orbital eccentricity alone is considered. In general more precision information about conductivity structure of planetary bodies e.g. separation of the thickness and conductivity of spherical body (or shell) would be expected to be given by multi-frequency sounding. Accordingly we forcus on subsolar distance as an index of the time variation of Mercury's external magnetic field in order to estimate the period characteristics of external field. Since magnetopause is determined by the balance between planetary intrinsic magnetic field and solar wind, subsolar distance is able to be regarded as an index of the variation of external magnetic field.

We identify the location of Mercury's magnetopause from vector magnetic field data by MESSENGER observation in fifteen Mercury years and study the period characteristics of Mercury's external magnetic field by converting the data of magnetopause into that of subsolar distance and analyzing the time-variation of them, and report the result.

Keywords: Mercury, MESSENGER, Magnetopause

Measurement of crater ray length by analysis of lunar images: A comparison with Z model

*Kinoshita Toshiki[1], Akiko Nakamura[1], Koji Wada[2]

1. Department of Planetology, Graduate School of Science , Kobe University, 2. Planetary Exploration Research Center, Chiba Institute of technology

The information of impactor, such as impact velocity, density, or radius, is coupled into a coupling parameter C (Holsapple and Schmidt, 1987) and cannot be resolved from crater diameter only. In order to examine if we can put constraints on the information of impactor by spatial extent of ejecta, i.e., the distribution of continuous ejecta and length of ray, we performed quantitative measurement of ejecta. We analyzed images provided by Multiband Imager (MI) onboard the JAXA’s lunar orbiter, Kaguya. We analyzed 13 small craters in the southwestern region of Kepler crater on Oceanus Procellarum. First, we tried to define the region to which we could apply Z model. We measured the circularity of the area with a reflectance higher than a set-value. In the figure, the horizontal axis shows the equivalent diameter of a circle of the region and the vertical axis shows the circularity. As the reflectance increases, the circularity of the region increases. The slope changes at the diameter roughly 4 times as large as the crater diameter. From this result, we regarded that the Z model is applicable to the region within about 4 crater radii from the crater center. In the region beyond about 4 crater radii, ejecta inelastically collided one another, became collimated in discrete directions, and deposited in rays (Kadono et al., 2015). In other words we assumed that the rays next to each other had shared the ejecta released in the direction in between. Based on this assumption, we calculate the thickness of ejecta in each ray using the angles between rays on the MI images, the width of rays, and Z model, and will discuss on its relationship with the crater diameter.

Keywords: crater ray, ejecta, Kaguya

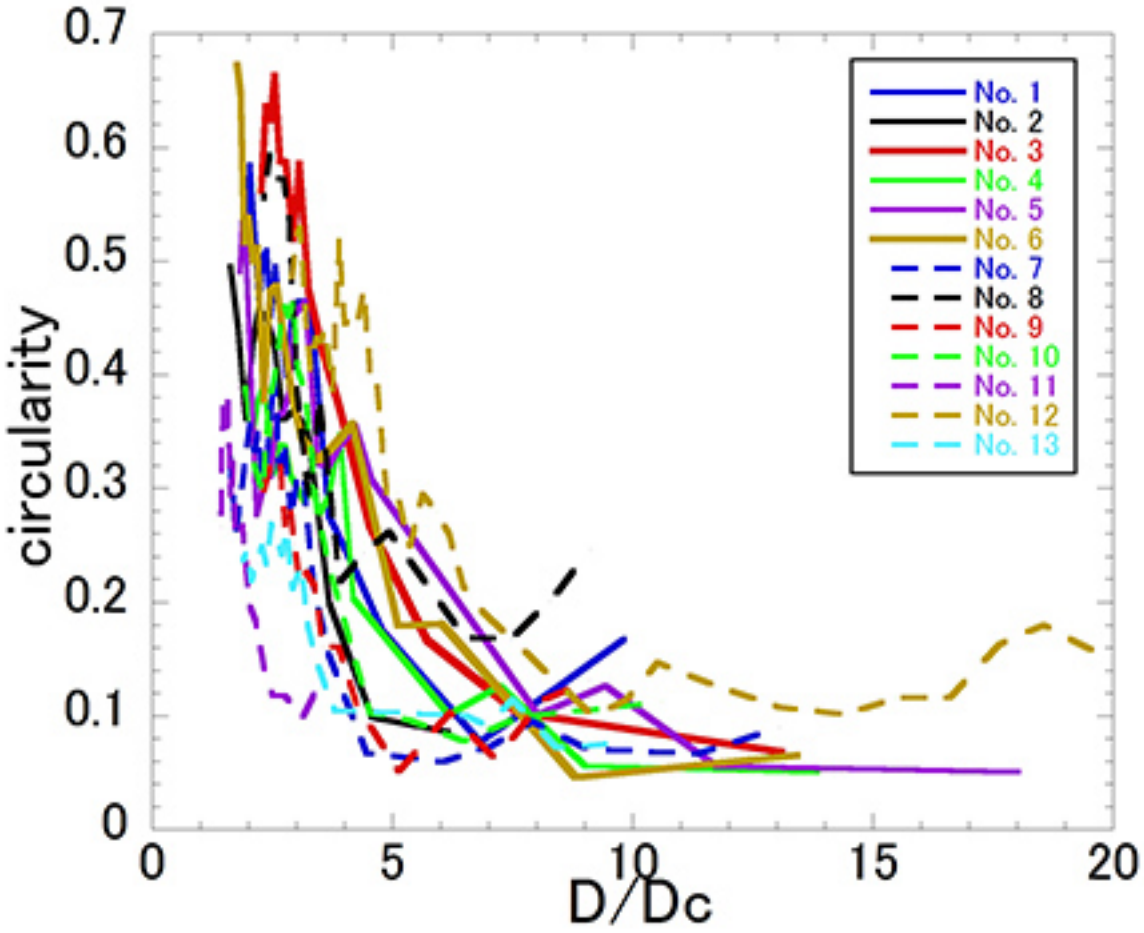

Correct correspondence selection between points on two asteroid images using epipolar constraint

*Junpei Ohyama[1], Naoya Ohta[1], Naoko Ogawa[2]

1. Gunma University, 2. Japan Aerospace Exploration Agency (JAXA)

In asteroid exploring missions like HAYABUSA 2, it is often needed to compute the shape of the target asteroid using its images taken after the space craft arrives at the asteroid. In this computation process, correspondences between points on two images taken from different view direction have to be established. In order to accomplish this task automatically, we first extract image features from the two images using image processing techniques, and compute matched pairs of them based upon similarity of the features. However, this similarity based matching produces relatively high rate of wrong correspondence. However, if we use epipolar constraint, which gives the relation between image positions of an object point on two images taken from different view points, it is expected that we can reduce the error rate of the correspondence. This report states the experimental results of this approach. In the experiments, we used images of an asteroid model made in JAXA, and AKAZE (Alcantarilla et al. 2013) as the image feature. The correct matches were selected by human eyes as the ground truth. In the case that the correct matching rate is 68 percents when using only the feature similarity, the correct matching rate increased to 97 percents when using epipolar constraint too. This result suggests using epipolar constraint is effective when establishing feature correspondence between two asteroid images.

Keywords: epipolar constraint, fundamental matrix, asteroid image, point correspondence, AKAZE

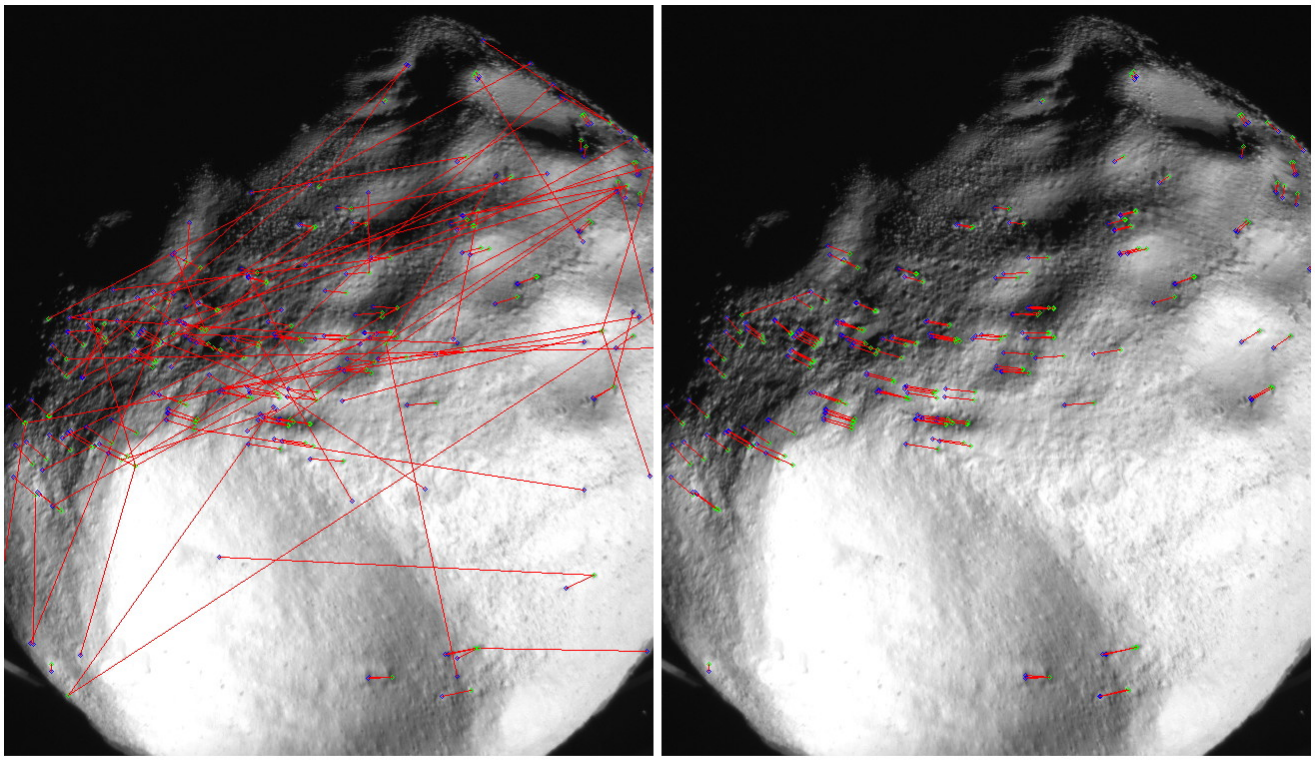

correspondances without epipolar constraint correspondances with epipolar constraint

Performance comparison between SIFT and AKAZE for corresponding point computation on asteroid images

*Hiroki Yamaguchi[1], Naoya Ohta[1], Naoko Ogawa[2]

1. Gunma University, 2. Japan Aerospace Exploration Agency (JAXA)

In asteroid exploring missions like HAYABUSA 2, it is often needed to compute the shape of the target asteroid using its images taken after the space craft arrives at the asteroid. In this computation process, correspondences between points on two images taken from different view direction have to be established. In order to accomplish this task automatically, image features computed by image processing techniques are used. Among many image features, it is reported that SIFT (Lowe 2004) has good performance for the current purpose (Takeishi et al. 2015). However, SIFT is protected by patent and this can be an obstacle for some situations. On the other hand, AKAZE (Alcantarilla et al. 2013), which was proposed after SIFT, has no limitation in its usage. So, we have compared the performances of SIFT and AKAZE when using them to asteroid images. In the experiments, images of an asteroid model made in JAXA were used. The number of feature points detected by SIFT (e.g. around 6000) is greater than that by AKAZE (e.g. around 3000), but even the number of points by AKAZE is enough amount for the current purpose. The error rates by SIFT and AKAZE for the correspondence computation between two images taken from different view angles are almost the same (e.g. 30 to 40 percents), and sometime the error rate by AKAZE becomes smaller the rate by SIFT (e.g. 32 vs. 36 persents). From these experimental results, we conclude AKAZE has enough performance for correspondence computation for asteroid images.

Keywords: SIFT, AKAZE, asteroid image, feature point, point correspondence

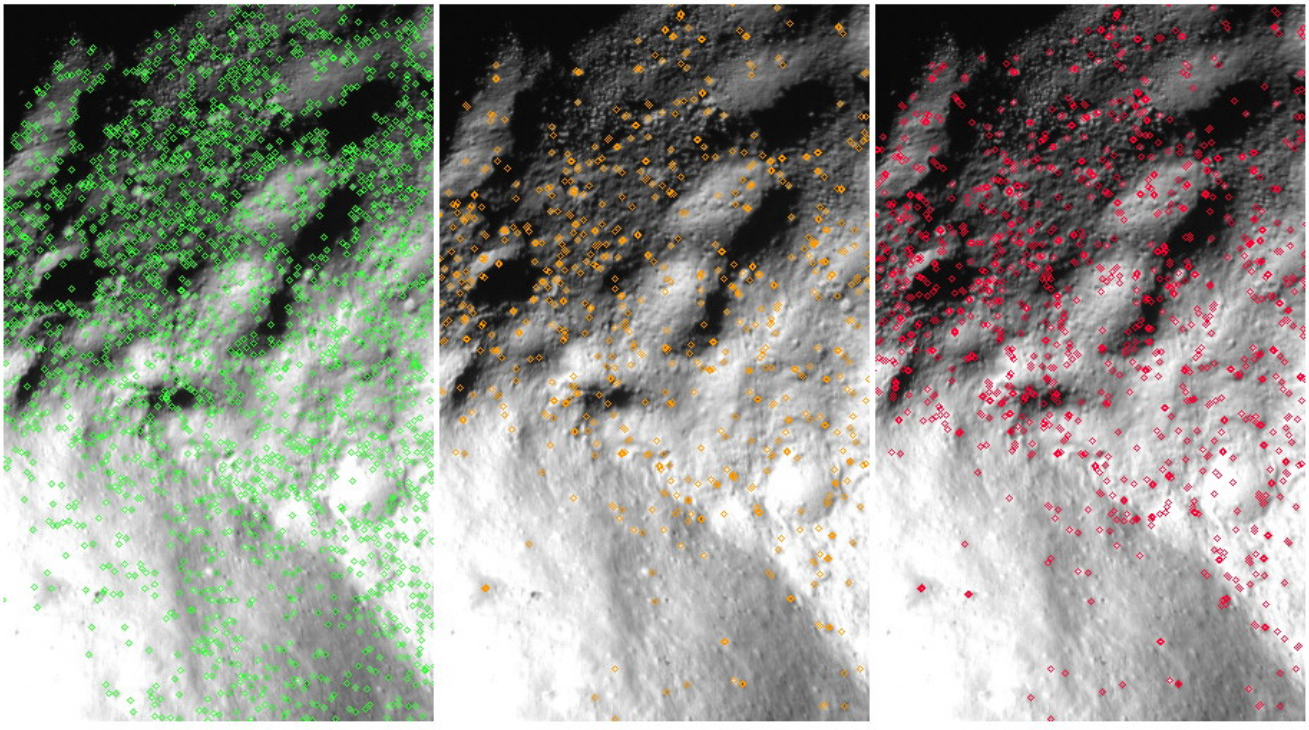

feature points by SIFT | common feature points | feature points by AKAZE

Near-Infrared Photometry of Near Earth Asteroid (1566) Icarus and 2007 MK6

*Yuri Sakurai[1], Seitaro Urakawa[2], Jun TAKAHASHI[3], Tomoyasu TANIGAWA[4], Sayuri NAKAMURA[5], George HASHIMOTO[1]

1. Department of Earth Sciences, Okayama University, 2. Japan Spaceguard Association, 3. University of Hyogo, 4. Sanda Shounkan Highschool, 5. Okayama University

Rotation period of Near Earth Asteroid (1566) Icarus is estimated to be 2.2726 hours (Warner, 2015). Since Icarus' rotation rate is just below the threshold for breakup via centrifugal force, breakup of Icarus might have occurred in the near past. Ohtsuka et al. (2007) found a dynamical relationship between Icarus and 2007 MK6, and proposed that 2007 MK6 is likely a family member of Icarus. To examine the Icarus' breakup hypothesis, we observed Icarus and 2007 MK6 at Nishi-Harima Astronomical Observatory with the Nishiharima Infrared Camera (NIC) which is a near infrared simultaneous three-band (J, H, and Ks) camera.
The observation of Icarus was done between 2015 June 18 and 21, and the observation of 2007 MK6 was done between 2016 June 15 and 18. For a flux calibration, we also observed nearby stars of spectral type G2V, and their magnitude were derived from the 2MASS database. The Icarus' breakup hypothesis was tested by a comparison of near infrared colors of Icarus and 2007 MK6.

Keywords: Asteroid, Photometry, Near-Earth Objects

Observation of near-earth object (1566) Icarus and the split candidate 2007 MK6

*Seitaro Urakawa[1], Katsutoshi Ohtsuka[2], Shinsuke Abe[3], Daisuke Kinoshita[4], Hidekazu Hanayama[5], Takeshi Miyaji[5], Shin-ichiro Okumura[1], Kazuya Ayani[6], Syouta Maeno[6], Daisuke Kuroda[5], Akihiko Fukui[5], Norio Narita[5,7,8], George HASHIMOTO[9], Yuri SAKURAI[9], Sayuri Nakamura[9], Jun Takahashi[10], Tomoyasu Tanigawa[11], Otabek Burhonov[12], Kamoliddin Ergashev[12], Takashi Ito[5], Fumi Yoshida[5], Makoto Watanabe[13], Masataka Imai[14], Kiyoshi Kuramoto[14], Tomohiko Sekiguchi[15], MASATERU ISHIGURO[16]

1. Japan Spaceguard Association, 2. Tokyo Meteor Network, 3. Nihon University, 4. National Central University, 5. National Astronomical Observatory of Japan, 6. Bisei Observatory, 7. Astrobiology Center, 8. University of Tokyo, 9. Okayama University, 10. University of Hyogo, 11. Sanda Shounkan Highschool, 12. Ulugh Beg Astronomical Institute Uzbekistan Academy of Science , 13. Okayama University of Science, 14. Hokkaido University, 15. Hokkaido University of Education, 16. Seoul National University

Background & Aim: A numerical simulation proposes that the origin of near-Earth object 2007 MK_6 (hereafter, MK6) is a near-Earth object (1566) Icarus (hereafter, Icarus) [1]. In addition to it, the orbital parameters of the daytime Taurid-Perseid meteor swarm are in good agreement with those of Icarus. Thus, it is considered that MK6 is split from the parent object Icarus by a rotational fission and/or an impact event, and the produced dust became to the daytime Taurid-Perseid meteor swarm. To confirm such a hypothesis, we need to obtain the observational evidence that the color indices of Icarus and MK6 are same. Moreover, if MK6 split by the rotational fission due to the YORP effect, the rotation period of Icarus would be shorten compared with the past rotation period. When the MK6 split by an impact event, the rotation period of MK6 would shorter than the spin limit of 2.2 hours. We require the observation for Icarus and MK6 to test these hypotheses.

Observations: We conducted the observations for Icarus in 2015 and MK6 in 2016, respectively. The observation summary is shown as followings: Icarus (June 2015): Nayoro Observatory 1.6 m Pirka telescope of the Hokkaido University (visible photometry), Ishigakijima Astronomical Observatory (IAO) 1.05 m Murikabushi telescope (g', R_C, and I_C band simultaneous photometry), Maidanak Observatory (MO) 0.6 m telescope (R band photometry), Nishi-Harima Astronomical Observatory (NHAO) Nayuta 2.0m telescope (J, H, and K_S band simultaneous photometry), Lulin and Kinmen Observatory 0.4 m telescopes (visible photmetry), Lowell Observatory (LO) 1.1 m, 1.8 m, and 4.3 m telescopes (visible photometry and visible spectroscopy), MK6 (June - July 2016): IAO 1.05 m Murikabushi telescope (g', R_C, and I_C band simultaneous photometry), MO 1.5 m telescope (R band photometry), NHAO Nayuta 2.0 m telescope (J, H, and K_S band simultaneous photometry), Lulin Observatory 1.0 m telescope (visible photometry), LO 1.8 m and 4.3 m telescopes (visible photometry and visible spectroscopy), University of Hawaii 2.24 m telescope (visible photometry), Okayama Astrophyscial Observatory 1.88 m telescope (g', r', and z' band simultaneous photometry).

Results: Previous studies indicated that the taxonomic type of Icarus is an S-type or a Q-type [2][3]. We obtained that the color indices $g' - R_C$ and $R_C - I_C$ are 0.828 ±0.027 mag and 0.397 ±0.025 mag, respectively. These are consistent with the color indices of an S-type asteroid. Moreover, the color indices implied the slight rotational color variation, though the further data analysis is needed. On the other hand, the color indices and the rotation period of MK6 have not been revealed in the previous study. In addition to the color indices of Icarus, we will present the result the color indices of MK6 and the rotation period of both Icarus and MK6.

References: [1] Ohtsuka K. et al. (2007) *ApJ*, *668*, L71-L74. [2]Chapman C. R., Morrison D., and Zellner B. (1975) *Icarus*, *25*, 104-139. [3]Hicks M. D., Fink U., and Grundy W. M. (1998) *Icarus, 133,* 69-78.

Keywords: Asteroids, Photometry, Near-Earth Objects

Sintering of icy dust aggregates due to turbulence in a protoplanetary disk

*Kiriko Kodama[1], Sin-iti Sirono[1]

1. Graduate School of Environmental Studies, Nagoya University

In a protoplanetary disk, coagulation of dust grains is the first step of planetary formation. It is important to know whether dust grains can grow or not. There are two types of dust grains. One is made of ice and the other of rock. In this study, we focus on icy dust grains. Icy dust aggregates are sintered when they are heated. Sintering is the material transfer phenomenon to decrease total surface area. When an icy dust aggregate is sintered, necks connecting dust grains grow. Because collision between sintered aggregates results in bouncing, they cannot grow. Hence, sintering greatly affects the first step of planetary formation.
The heat source is visible light irradiation from the central star in a protoplanetary disk. Because the dust grains around at the midplane blocks the irradiation, only dust grains around the surface of a disk can be heated. Therefore, if turbulence transports an icy dust aggregate to the surface having high temperature, sintering can proceed.
Using radial temperature distribution at the midplane, a timescale required for sintering was estimated by Sirono (2011, ApJ, 735, 131). However, this study did not take account of the vertical motion of icy dust aggregates. In this study, we calculate the vertical motion of each aggregate to clarify the sintering timescale shortened by turbulent diffusion.
The vertical motions of dust aggregates are diffusion by turbulence and sedimentation by gravity of the central star. Distribution of dust aggregates reaches a steady state in the sedimentation timescale. In the steady state condition, each aggregate moves up and down in a vertical direction of a protoplanetary disk, icy dust aggregates are sintered if they exceed the altitude of high temperature. We calculated the position of aggregates as a function of time. Because sintering strongly depends on temperature (Sirono, 2011, ApJ, 735, 131), sintering of icy dust aggregates can be assumed to quickly proceed at a particular height from the midplane. By numerical simulation we calculated the fraction of sintered dust aggregates that experienced high temperature. The fraction of sintered dust aggregates increases with time. From this fraction, the sintering timescale is determined.
It is found that the sintering timescale gets shorter as the altitude of high temperature decreases. If it falls to the dust aggregate disk scale height, the sintering by turbulent diffusion proceeds enough. The altitude of high temperature depends on opacity of aggregates. If the opacity goes down as dust aggregates grow, the new sintering region appears. However, if a little small dust aggregates are present, the height can hardly fall down. Therefore, the sintering by transporting to disk surface does not proceed.

Keywords: protoplanetary disk, sintering, turbulence

Distribution of captured planetesimals in circumplanetary disks and implications for accretion of regular satellites

*Ryo Suetsugu[1], Keiji Ohtsuki[2]

1. University of Occupational and Environmental Health, 2. Kobe University

Regular satellites of giant planets are formed by accretion of solid bodies in circumplanetary disks. Planetesimals that are moving on heliocentric orbits and are sufficiently large to be decoupled from the flow of the protoplanetary gas disk can be captured by gas drag from the circumplanetary disk. In the present work, we examine the distribution of captured planetesimals in circumplanetary disks using orbital integrations. We find that the number of captured planetesimals reaches an equilibrium state as a balance between continuous capture and orbital decay into the planet. The number of planetesimals captured into retrograde orbits is much smaller than those on prograde orbits, because the former ones experience strong headwind and spiral into the planet rapidly. We find that the surface number density of planetesimals at the current radial location of regular satellites can be significantly enhanced by gas drag capture, depending on the velocity dispersions of planetesimals and the width of the gap in the protoplanetary disk. Using a simple model, we also examine the ratio of the surface densities of dust and captured planetesimals in the circumplanetary disk, and find that solid material at the current location of regular satellites can be dominated by captured planetesimals when the velocity dispersion of planetesimals is rather small and a wide gap is not formed in the protoplanetary disk. In this case, captured planetesimals in such a region can grow by mutual collision before spiraling into the planet, and would contribute to the growth of regular satellites.

Keywords: planets and satellites

Temporary Capture of Small Bodies by an Eccentric Planet

*Arika Higuchi[1], Shigeru Ida[2]

1. Tokyo Institute of Technology, 2. Earth-Life Science Institute

We have investigated the probability of temporary capture of asteroids in eccentric orbits by a planet in a circular or an eccentric orbit by analytical and numerical calculations. We found that in the limit of the circular orbit, the capture probability is ~0.1% of encounters to the planet's Hill sphere, independent of planetary mass and semimajor axis. In general, the temporary capture becomes difficult, as the planet's eccentricity (e_p) increases. We found that the capture probability is almost independent of e_p until a critical value (e_p^c) that is given by ~5 times of Hill radius scaled by the planet's semimajor axis. For $e_p > e_p^c$, the probability decreases approximately in proportional to e_p^{-1}. The current orbital eccentricity of Mars is several times larger than e_p^c. However, since the range of secular change in Martian eccentricity overlaps e_p, the capture of minor bodies by the past Mars is not ruled out.

Keywords: Martian moons, asteroids

Position of Snow Line Depending on Spatial Distribution of Magnetorotational Instability in Protoplanetary Disks

*Shoji Mori[1], Satoshi Okuzumi[1]

1. Department of Earth and Planetary Sciences, Tokyo Institute of Technology

Icy dust plays important role of planetesimal formation in protoplanetary disks because it dominates mass of the solid material. In addition, because icy dust is also related to origin of ocean of rocky planets, to understand spatial distribution of icy dust is essential for not only planet formation but also origin of life. Icy dust is present beyond sublimation boundary of H^2O ice (snow line). Therefore, to understand radial temperature profile which determines position of snow line is particularly important. Before the disk dissipating, at the inner region in which snow line lies is optically thick, gravitational energy of accreting gas is converted by turbulent viscosity to heat accumulated onto the disk. The heat determines the temperature profile. That is this viscous heating controls the position of snow line (Oka et al. 2011).

The turbulence in protoplanetary disks is driven by an instability (magnetorotational instability) caused by interplay between disk magnetic fields and ionized gas. Growth of magnetorotational instability causes vigorous turbulence, although it needs sufficient ionization fraction of the disk. Therefore, at high density region of too low ionization fraction, magnetorotational instability is stable. In that region, magnetic turbulence would not be generated.

When one considers the viscous heating, heating rate distribution concentrating on midplane is often assumed. However, in the stable region, because absence of turbulence, the turbulent viscosity generates heat at the upper layer (Hirose & Turner 2011). Since viscous heating increases the midplane temperature by accumulation of heat into optically thick region, heat at the upper layer leads to lower midplane temperature than heating at midplane.

In this work, focusing on this fact, we investigate temperature profile based on distribution of magnetic turbulence and the position of snow line. Specifically, we perform three dimensional magnetohydrodynamics simulation including stratification and ionization fraction distribution. As a result, we confirm that peak of the heating rate is located at 3 scale height from midplane. This is consistent with Hirose & Turner (2011). We calculate the position of snow line assuming the accreting heating releases at 3 scale height. As a result, in the case of accretion rate of 10^{-8} M_{solar}/year, snow line of 3 AU with midplane heating changes to snow line of 0.7 AU with upper layer heating. Thus, the distribution of magnetic turbulence would control position of snow line. We also investigate dependence of initial magnetic field strength on the dissipation rate distribution and discuss the position of snow line depending on the initial magnetic field strength.

Keywords: Protoplanetary disk, Magnetohydrodynamics, Snow line

Numerical simulation of Saturn ring formation using SPH

*keiya murashima[2], Natsuki Hosono[1], Yosuke Yamashiki[1]

1. Global Water Resources Assessment Laboratory - Yamashiki Laboratory Graduate School of Advanced Integrated Studies in Human Survivability Kyoto University, 2. Faculty of Science, Kyoto University

The origin of Ring formation of Saturn is well explained by Ripped-apart icy moon hypothesis proposed by Canup et al.,in which Saturn's planetary tidal forces preferentially strip material from the Titan-sized icy moon’ s outer icy layers, while its rocky core remains intact and is lost to collision with the planet.
We performed numerical simulations using SPH and surveyed the effect of the initial conditions and dependance of the number of particles to the results. We will show the the result of numerical simulations which includes the material strength.

Keywords: Ripped-apart icy moon, SPH, propeller structure

Ring formation around giant planets by tidal disruption of a passing large Kuiper belt object

*Ryuki Hyodo[1,2,3], Sebastien Charnoz[2], Keiji Ohtsuki[3], Hidenori Genda[1]

1. Earth-Life Sicence Institute, Tokyo Institute of Technology, 2. Institut de Physique du Globe de Paris, 3. Graduate School of Science, Kobe University

The origin of rings around giant planets remains elusive. Saturn's rings are massive and made of 90–95% of water ice with a mass of ~10^{19} kg. In contrast, the much less massive rings of Uranus and Neptune are dark and likely to have higher rock fraction. According to the so-called “Nice model”, at the time of the Late Heavy Bombardment, giant planets could have experienced a significant number of close encounters with bodies scattered from the primordial Kuiper Belt. This belt could have been massive in the past and may have contained a larger number of big objects ($M_{body}=10^{22}$ kg) than what is currently observed in the Kuiper Belt. Here we investigate, for the first time, the tidal disruption of a passing object, including the subsequent formation of planetary rings. First, we perform SPH simulations of the tidal destruction of big differentiated objects ($M_{body}=10^{21}$ and 10^{23} kg) that experience close encounters with Saturn or Uranus. We find that about 0.1–10% of the mass of the passing body is gravitationally captured around the planet. However, these fragments are initially big chunks and have highly eccentric orbits around the planet. In order to see their long-term evolution, we perform N-body simulations including the planet's oblateness up to J_4 starting with data obtained from the SPH simulations. Our N-body simulations show that the chunks are tidally destroyed during their next several orbits and become collections of smaller particles. Their individual orbits then start to precess incoherently around the planet's equator, which enhances their encounter velocities on longer-term evolution, resulting in more destructive impacts. These collisions would damp their eccentricities resulting in a progressive collapse of the debris cloud into a thin equatorial and low-eccentricity ring. These high energy impacts are expected to be catastrophic enough to produce small particles. Our numerical results also show that the mass of formed rings is large enough to explain current rings including inner regular satellites around Saturn and Uranus. In the case of Uranus, a body can go deeper inside the planet's Roche limit resulting in a more efficient capture of rocky material compared to Saturn's case in which mostly ice is captured. Thus, our results can naturally explain the compositional difference between the rings of Saturn, Uranus and Neptune.

This work is published in Hyodo,R.,Charnoz,S.,Ohtsuki,K.,Genda,H. 2017, Icarus, 282, 195-213.

Keywords: Rings, Satellites, Giant planets

Effect of Planetary Spin on Giant Impacts

*Natsuki Hosono[1,2], Eiichiro Kokubo[3]

1. Kyoto University, 2. RIKEN, 3. NAOJ

In planetary science, impact phenomena between two objects play an important role, e.g., the Moon-forming impact.
Thus, to date, a lot of numerical simulations of giant impacts are carried out.
A potentially important effect on giant impacts is the spin of colliding bodies.
However, most previous works neglected the spin.
It is more natural that the bodies have pre-impact rotations.
In this work, we systematically investigate the effect of the spin on giant impacts.
We employ the Density Independent SPH, which is an improved version of the standard SPH method.
We show the dependence of the collisional outcome on the spin period.

The Origin of Asteroid Geometries: Dependence on Conditions of Planetesimal Collisions

*Keisuke Sugiura[1], Shu-ichiro Inutsuka[1], Hiroshi Kobayashi[1]

1. NAGOYA UNIVERSITY Graduate School of Science

Recent observations by space probes or light curves clarify that most of asteroids in present solar system have irregular shapes distinctly different from a sphere, such as asteroid Itokawa. These irregular shapes are supposed to be created by collisional destruction and coalescence of planetesimals. We expect that we can clarify the past environment of the solar system if we clarify the relationship between impact condition, such as impact angle or velocity, and resultant irregular shape of planetesimal, and compare with the asteroid shapes in present solar system.
For relatively small objects like planetesimals, effect of material strength or friction is also important other than effect of the self-gravity. To investigate the resultant shape of planetesimals made by collisional destruction and re-accumulation, we developed numerical simulation code of Smoothed Particle Elastic Dynamics (Sugiura and Inutsuka 2016, 2017). Moreover, we included fracture model (Benz and Asphaug 1995) and friction model (Jutzi 2015) to describe realistic property of rocks. Owing to friction model, we can represent the irregular shape of rubble pile formed by re-accumulation of fragments. Our simulation code also calculates the self-gravity, and thus we can treat collisional destruction and subsequent gravitational re-accumulation consistently.We simulate the collision between rocky planetesimals with the radius of about 50 km while varying the impact velocity, impact angle and mass ratio, and we measure the axis ratios of fragments with sufficiently high resolution. In this talk, we will discuss the relationship between resultant shape of planetesimals and impact condition, and mechanism to produce irregular shapes.

Keywords: asteroid geometry, planetesimal collision, SPH, elastic dynamics

Impact cratering on a silica dust layer with high porosity and the effect of porosity on the crater size scaling law

*Takuya Ishiguro[1], Masahiko Arakawa[1]

1. Graduate School of Science, Kobe University

Recent planetary exploration revealed that small bodies in the solar system could have a large porosity as large as 80% for comet nuclei and less than 75% for asteroids. Impact craters found on such highly porous bodies were recognized to be quite different from that found on rocky bodies without porosity, that is, there were several craters on their surface which sizes were beyond their radius. These large craters were supposed to be formed by pore collapse during the impact compression and so it was recently classified into a compressive type crater. Classically, the impact crater is classified into two types depending on the physical mechanism controlling the final crater size: they are a crater formed in a gravity dominated regime and a crater formed in a strength dominated regime. These classical type crates have been studied to construct the crater size scaling law, and now the p scaling law was widely accepted to use for the planetary impact phenomena. However, the effect of porosity on this p scaling law for the crater size was not clarified yet although limited studies have been conducted by Housen and Holsapple (2003) and others. The π scaling law applicable for the porous asteroids is necessary for the impact experiment on small asteroid Ryugu by Hayabusa-2 small carry-on impactor because one candidate for the surface condition on Ryugu is fine-grained layer with a high porosity.
In this study, commercial amorphous silica dusts with the average particle size of 0.5mm and the density of 2.2gcm^{-3} (ρ) were used to prepare the target with the bulk porosity from 50% to 78%, and the target was simply consolidated by the cohesion force of Van Der Waals force with the tensile strength from 100 Pa to 10^4 Pa. We made impact cratering experiments using this porous target to study the effect of the porosity on the crater morphology including the crater size. Impact experiments were conducted by using a horizontal type two-stage light gas gun set at Kobe University and a glass bead projectile with the diameter of 2mm and the mass of 10 mg (m_p) was launched at the impact velocity at 3.60 kms^{-1}. The projectile was impacted on the target surface normally set in a large vacuum chamber less than 20 Pa. The crater morphology was found to change with the increase of the porosity, that is, the shallow dish type crater was observed on the target with the porosity of 50% having the tensile strength of 10^4 Pa, and as the porosity increased the impact spherical cavity was formed to grow and expanded below the shallow dish crater. The recovered target was hardened by epoxy resin and cut at the center of the crater to observe the cross section to measure the cavity diameter (D), the depth of the crater (d) and the diameter of the shallow dish crater. The relationship between the distension ($a=\rho / \rho_{bulk}$) and the normalized cavity diameter, $\pi_D=(\rho_{bulk} D/m_p)^{1/3}$, was found to follow the empirical equation of $\pi_D=3.8a^{0.7}$, where r_{bulk} is bulk density of the target, and the relationship between the distension and the normalized depth, $\pi_D=(\rho_{bulk} d/m_p)^{1/3}$, was found to follow the empirical equation of $\pi_D=3.0a^{1.0}$. While the crater diameter of the shallow dish crater found at the entrance of the cavity was recognized to be constant irrespective of the porosity. These empirical equations could be used to incorporate the effect of porosity on the crater size scaling law.

Keywords: Impact crater, scaling law, porous bodies

Probability distribution of impact strength on the target simulating meteorites and implication for the size dependence of asteroid strength

*Fumiya Nagatomo[1], Masahiko Arakawa[1], Chisato Okamoto[1]

1. Graduate School of Science, Kobe University

Impact strength of asteroids is one of the most important physical parameter to control the size frequency distribution of asteroids in the main belt. The impact strength has been studied in the laboratory using cm-scale targets simulating various type asteroids such as rocky, icy and metal bodies, and these previous studies revealed that the impact strength strongly depended on materials and internal structure such as porosity. However, actual collision among asteroids happen at the scale of several orders of magnitude larger than that at the laboratory scale. Therefore, the size dependence of the impact strength is quite important to consider the asteroid collision. There is a traditional theory for material strength and it is well known that the material strength follows probability distribution: it scatters according to Weibull distribution. This probability distribution of the material strength is theoretically connected to the size dependence of the material strength: so called the Weibull statistical fracture theory. This size dependence is confirmed at the static deformation condition so far, then we try to extend this Weibull theory to the dynamic deformation condition corresponding to high-velocity impact for the purpose of asteroid collisions.

We made impact disruption experiments by using a vertical type gas gun set at Kobe University. A nylon ball projectile with the diameter of 10mm was launched at the velocity from 65 to 208 ms^{-1}, and was impacted on the target surface normally. The targets were a gypsum-glass beads mixture (GG) with the mean density of 1.9gcm^{-3} or a gypsum-bentonite mixture (GB) with the mean density of 0.77 gcm^{-3}; both had a shape of cylinder whose dimeter was 30mm. CG and GB targets were analogues of chondritic meteorites, so the glass beads with the size of 1mm simulated a chondrule. The impact experiments were conducted 10 times at the same impact condition for each target: the constant energy density (Q: the kinetic energy of projectile divide by target mass) was applied to the target, and we measure the mass of the largest fragment (LFM) at each time, then we noticed that the resultant 10 data were so scattered. We studied the probability distribution of the largest fragment mass, and then we obtained the impact strength (Q^*) from the largest fragment mass on the basis of the typical relationship between LFM and Q. Impact experiments at two different energy densities were conducted for each target. We also measured the tensile strength of GG and GB targets more than 10 times by the static deformation test to study the probability distribution of the tensile strength.

We obtained the Weibull parameter (Φ) to characterize the probability distribution of the strength for the tensile fracture: Φ=7 and 8 for GG and GB target, respectively; they are similar to the values obtained for basalt and granite. The cumulative probability, P, of the fracture for the materials is shown as follows according to the Weibull theory, $P=1-\exp(-V/V_0(\sigma/\sigma_0)^{\Phi})$ (eq.1), where V is volume of the target and σ is strength, and the suffix 0 shows the standard condition. The largest fragment mass recovered from impact experiments was found to scatter so much; e.g. GG target showed the scattering in one order of magnitude. The average impact strength of GG and GB target for 20 experiments in each was obtained to be 34 and 158 Jkg^{-1}, respectively, and we tried to make the relationship between P and Q^* according to eq.1 by substituting Q^* for σ, where Q^* was determined from each LMF using the typical relationship between LFM and Q, then $\Phi$was obtained from the probability distribution of the impact strength: $\Phi$is 1.8 and 2.6 for GG and GB target. Thus, the size dependence of the impact strength could be estimated from

eq.1 setting P=0.5: $Q^*=Q_0 D^{-n}$, where D is the target size and n is 1.6 and 1.2 for GB and GG target, respectively.

Keywords: Impact strength, Impact scaling law, Asteroids

High-velocity impact cratering experiments on granular layer with various water contents

*Taku Tazawa[1], Masahiko Arakawa[1], Kazuma Matsue[1]

1. Graduate School of Science, Kobe University

Recent study on numerical simulations of large scale impact cratering showed that complex crater such as a central-peak type crater was formed within the region where the materials composing the surface crust lost their shear strength by high shock pressure, and that this fluidized region should have a rheological property like Bingham fluid: it has a finite yield strength and behaves as Newtonian fluid beyond the yield strength. Although there are a lot of studies on the large scale complex craters by numerical simulations by using iSLAE, there is little studies to compare these simulations with laboratory experiments. Thus, the numerical results should be confirmed by the laboratory experiments to assure their numerical models. One of the most important points of the numerical model is rheological properties of the fluidized region and how it behaves during the crater formation process. Then, we try to study the crater formation process of fluidized material with various rheological properties such as yield strength and viscosity.
In this study, we used granular materials including various water contents in order to control the rheological properties of target. Glass beads with the size of 100 μm and quartz sand with the size of 100 μm were used for the target with the water contents from 0 to 24.5 wt.%, and we found that the pore space in the granular layer was completely filled with water at the content larger than 19.3 wt.%. The yield strength, Y, of the wet glass beads layer was measured by means of indentation tests and the obtained Y rapidly increased from 1kPa to 50kPa when the water content changed from 0 to 3wt.%, then it gradually increased from 50kPa to 100kPa until 17.5wt.%. Beyond the content of 17.5wt.%, the Y suddenly dropped below 5kPa until 19.5wt.%. Moreover, the relationship between the Y and the indentation speed for the wet glass beads layer with the content of 20wt.% was studied, and it was clarified that the Y of this saturated layer was proportional to the square root of indentation speed. We used this wet glass beads with various rheology for the high-velocity cratering experiments. The impact experiments were made by using a vertical type gas gun set at Kobe University, and the target box was set below a wind shield in a sample large chamber. The glass bead projectile with the size of 3mm was launched at the velocity of 170m/s, and the cratering process was observed by a high-speed digital video camera with the frame rate of $2x10^3$ FPS.
The crater shape was found to change with the water content: a bowl type for 0 to 3wt.%, a pit type with fractured rim for 3wt.% to 17.5wt.%, and a pit type with deformed rim for > 17.5wt.%. The high speed camera image was used to characterize the ejecta corresponding to the crater morphology. The bowl type crater was associated with a continuous ejecta curtain, and the pit type crater with a fractured rim was associated with many fragments composed of clumps. The pit type crater with a deformed rim formed small amount of ejecta and was associated with low velocity ejecta curtain undetached from the surface. The crater diameter was found to monotonically decrease with the water contents up to 18.3wt.% irrespective of the crater morphology, but the crater depth decreased until 15wt.% and then it rapidly increased from 15wt.% to 18.3wt.% corresponding to the pit type crater with a deformed rim. Thus, the depth to the diameter ratio could be classified into 3 region depending on the crater morphology: it simply increased from 0.1 to 0.5 for a bowl type, and it was a constant of 0.5 for a pit type with a fractured rim, and then it rapidly increased again for a pit type with a deformed rim. The crater depth could be controlled by the yield strength of the wet sand, but the crater diameter could not be controlled by the yield strength at the water content larger than 17.3wt.%. In this region, the wet sand showed non-newtonian behavior, thus this rheological property might cause the decrease of the crater diameter in

this region.

Keywords: Complex crater, Rheology, High-Velocity impact phenomena

The effect of sulfur on space weathering

*Hirokazu Tanaka[1], Sho Sasaki[1], Mizuki Okazaki[1], Takahiro Hiroi[2]

1. Department of Earth and Space Sciences, School of Science, Osaka University , 2. Department of Earth, Environmental and Planetary Sciences, Brown University

Space weathering alters surface optical properties on airless rocky bodies; the spectral darkening, reddening, and weakening of absorption bands are shown as for the optical changes. The cause of these changes is nanophase iron particles (np) generated by irradiation of solar wind or bombardment of micrometeorites. Although space weathering is also observed on the surface of Mercury, Messenger showed that there was a little iron, which was the main driver of space weathering, while there was more sulfur in weight abundance. Not only np but also sulfur or its compounds would contribute to space weathering. Okazaki et al. (2016) showed that addition iron sulfide to olivine samples had the effect of promoting space weathering. Moreover, SEM observation suggests that there is sulfur deposition on an olivine particle and which causes Mercury-like space weathering. In this study, we irradiated laser to the sample containing pure sulfur in order to simulate and examine the effect of sulfur on space weathering. First, we performed experiments of pulse laser irradiation to olivine and S mixture samples in a vacuum chamber. The samples were made with olivine and 10 weight % of S mixture (both particle size 45-75 m), and they were irradiated at 5 mJ. Moreover, we carried out additional thermal fatigue experiments to some of laser irradiated sample. After laser irradiation and/or thermal fatigue experiments, reflectance spectra (wavelength range 250-2500 nm) of these samples were measured by a spectrometer in order to examine alteration in optical properties.
The result of laser irradiation experiments showed that the spectra of samples including S reddened more than those without S. The result of thermal fatigue experiments showed that the spectra of samples including S changed complexly going with vaporization loss of S. It is confirmed that sulfur influence changes of optical properties in space weathering.

Performance report of solar wind ion irradiation equipment

*Yusuke Nakauchi[1], Toru Matsumoto[2], Masanao Abe[2,1], Akira Tsuchiyama[3], Aki Takigawa[3,5], Naoki Watanabe[4], Yuma Asada[3]

1. The Graduate University for Advanced Studies, 2. The Japan Aerospace Exploration Agency, 3. Kyoto University, 4. The Hakubi Center for Advanced Research, Kyoto University, 5. Hokkaido University

For understanding the evolution of the solar system, the material distribution in the early solar system is important. Meteorites provide large information on materials of the solar system, but they do not retain direct evidences for which parent body each meteorite came from.
The comparison between reflectance spectra of asteroids and meteorites suggest that the origins of almost all meteorites are asteroids. However, there are clear differences between reflectance spectra of asteroids and meteorites [references], which may be due to the space weathering on the surfaces of the asteroids. Recent studies proposed the importance of the influence of the solar wind implantation on the asteroidal surfaces in the near-Earth orbit [e.g. 1, 2]. Solar wind is composed of ~95% hydrogen, ~4% helium and other atoms [3]. However, space-weathering effects by low energy proton and helium ions consisting of the solar wind have not been understood well. In this study, we established ion beam irradiation equipment in ISAS/JAXA. This equipment is composed of an ion gun, main chamber (ion irradiation room), load lock chamber (sample preparation and FTIR measurement room), and FTIR. We can select ions with a specific mass and valence using the electric and magnetic fields. The maximum acceleration energy of ions is 5 keV. The reflection spectra of the irradiated samples can be measured without exposing the sample to the atmosphere. The optical path of FTIR can be purged with nitrogen. Therefore, the FTIR spectra of irradiated samples are obtained with minimized influences of adsorbed water and atmospheric fluctuations. In this presentation, we report the performance (e.g. beam current, beam shape) of ion beam irradiation equipment.

[1] C.M. Pieters et al., Science, 326(5952):568–572, 2009.
[2] T. Noguchi et al., MPS, 49(2):188–214, 2014.
[3] J.T. Gosling, Encyclopedia of the Solar System (Second Edition), pages 99 –116, 2007.

Keywords: solar wind, space weathering

Development of Exoplanet Observation System using ExoKyoto

Yosuke Yamashiki[1], Takao Doi[3], *Takanori Sasaki[2], Akihiro Yamanaka[5], Yuuki Saito[5], Shigeru Namiki[5], Keiya Murashima[5], Natsuki Hosono[1], Shota Notsu[2], Yuta Notsu[2], Kuroki Ryusuke[1], Hiroaki Sato[4], Fuuka Takagi[6]

1. Global Water Resources Assessment Laboratory - Yamashiki Laboratory Graduate School of Advanced Integrated Studies in Human Survivability Kyoto University, 2. Graduate School of Science, Kyoto University, 3. KYOTO UNIVERSITY UNIT OF SYNERGETIC STUDIES FOR SPACE, 4. Faculty of Engineering, Kyoto University, 5. Faculty of Science, Kyoto University, 6. Faculty of Agriculture, Kyoto University

An integrated database of confirmed exoplanets has been developed and launched as “ExoKyoto,” for the purpose of better comprehension of exoplanetary systems in different star systems. The HOSTSTAR module of the database includes not only host stars for confirmed exoplanets, but also over hundred thousands of stars existing in the star database listed in (HYG database). Each hoststar can be referred to in the catalogue with its habitable zone calculated, based on the observed/estimated star parameters. For outreach and observation support purpose, ExoKyoto possesses Stellar Windows, developed by the Xlib & Ggd module, and interfaces with GoogleSky for easy comprehension of those celestial bodies on a stellar map. Target stars can be identified and listed by using this database, based on the target magnitude, transit frequency, and photon decrease ratio by its transit. Using the developed exoplanet observation system on ExoKyoto, we performed some test observations at Kwasan Observatories, Kyoto University. We will show some preliminary results of the observations and introduce how to use the exoplanet observation system using ExoKyoto.

Extrasolar Planet’s Catalogue (ExoKyoto)
http://www.exoplanetkyoto.org

Keywords: Extrasolar Planets, Exoplanetkyoto, habitable zone

Atmospheric Dynamics on Non-Synchronized Tilted Exoplanets: Implications on Observed Thermal Light Curves

*Kazumasa Ohno[1], Xi Zhang[2]

1. Department of Earth and Planetary Science, Tokyo Institute of Technology, 2. Department of Earth and Planetary Science, University of California Santa Cruz

Various theoretical studies of atmospheric dynamics have investigated the dynamical structure on close-in synchronized exoplanets and succeeded to explain the phase curve observations. As the planets are farther away from their central stars, they are not likely to be tidally locked. Recent studies also begin to examine the atmospheric dynamics on non-synchronized exoplanets (e.g., Showman et al. 2015); however, they assume the planetary obliquity, the angle between orbital normal and planetary spin axis, is zero that is usually not true for non-synchronized planets.

In this study, we investigated the atmospheric dynamics on non-synchronized tilted exoplanets with a 2D general circulation model. We find that the temperature structure is considerably different from that on the synchronized exoplanets. Non-zero obliquities induce the temperature structure that is dominated by diurnal mean insolation if the radiative timescale is longer than rotation period but shorter than orbital period. The temperature is dominated by annual mean insolation if the radiative timescale is longer than both rotation and orbital periods. Seasonal variation as function of orbital phase is analyzed. We also predict the shape of observed thermal light curves for non-synchronized tilted exoplanets. Our prediction suggests that the amplitudes of light variation for high-obliquity exoplanets might be several times larger than that for the low-obliquity exoplanets but the differences depend on the parameters such as the radiative timescale and the line of sight from an observer. Furthermore, we find that the thermal light curves for tilted exoplanets might have a peak after the secondary eclipse if they are transiting, whereas for synchronized planets the phase curve peak always occurs before the secondary eclipse. Consequently, our results suggest that the planetary obliquity has the crucial impacts on the interpretations of observed phase curves for non-synchronized exoplanets.

Keywords: Exoplanets, Atmospheric Dynamics, Thermal Light Curve

Equilibrium chemical structure of extrasolar gas giant planets with various elemental abundance and temperature profiles

*Shota Notsu[1], Hideko Nomura[2], Catherine Walsh[3], Christian Eistrup[4]

1. Department of Astronomy, Graduate School of Science, Kyoto University, 2. Department of Earth and Planetary Science, Tokyo Institute of Technology, 3. School of Physics and Astronomy, University of Leeds, UK, 4. Leiden Observatory, Leiden University, The Netherlands

It is thought that difference in snowlines of oxygen- and carbon-bearing molecules, such as H_2O, CO, HCN, CO_2, will result in systematic variations in the C/O ratio both in the gas and ice. In addition, the C/O ratio of atomosphere of some exoplanets (e.g., Hot Jupiter) were measured by recent studies (e.g, Madhusudhan et al. 2011). Therefore, the planet forming regions could be confined through comparing the radial distributions of C/O ratio in disks and those of planetary atmospheres (e.g., Oberg et al. 2011, Eistrup et al. 2016).

In previous studies, We have calculated the chemical composition and the molecular line profiles in various protoplanetary disks, and have identified candidate molecular lines ranging from infrared to sub-millimeter wavelengths to locate the position of snowlines and C/O ratio distributions through future spectroscopic observations (e.g., Notsu et al. 2016, ApJ, 827, 113; 2017, ApJ, 836, 118).

In this study, first we calculated the physical structure of irradiated extrasolar gas giant planets using the analytic radiative equilibrium model in Guillot et al. (2010, A&A, 520, A27). Then, we calculated the chemical structure on equilibrium state of the gas giant planets. In these chemical calculations, we adopted various values of the distance from the central star, and elemental abundance (e.g., C, O, N), in order to investigate the relations between chemical structure of planetary atmospheres and their formation conditions in protoplanetary disks.

We found that as the values of temperatures in planetary atmosphere become smaller, the abundance of CH_4 become higher. In addition, as the values of C/O ratio become larger than the solar value, the abundance of CH_4 and HCN become higher in the lower atmospheres. In our talk, we will introduce the present calculational results, and will briefly comment the relations between the calculational results and recent observations.

Keywords: Extrasolar planet, Gas planetary atmosphere, Chemical equilibrium, C/O ratio, Snowline, Protoplanetary Disk

Simulation of the early Martian climate using a general circulation model, DRAMATIC MGCM: Impacts of thermal inertia

*Arihiro Kamada[1], Takeshi Kuroda[2], Yasumasa Kasaba[1], Naoki Terada[1]

1. Graduate School of Science, Tohoku University, 2. National Institute of Information and Communications Technology

There are many fluid traces on the Martian surface supposed to be made before ~3.8 billion years ago. If they were made by the liquid H_2O, the environment of the ancient Mars should be suitable for huge amount of liquid water, at least under higher temperature and larger atmospheric pressure than today. In order to reproduce such early Martian climate, several modeling studies have been performed so far. The solar insolation at that time is thought to be ~75% of today from a standard stellar evolution model. In this condition, a preceding study using the LMD Martian General Circulation Model (MGCM), with vertical 15 layers up to ~50 km altitude assuming the pure CO_2 atmosphere, showed that the surface temperature above 273 K could not be reproduced in the range of the surface pressure in 0.1 - 7 bars [Forget et al., 2013, hereafter F13], which is so-called the 'Early faint Sun paradox'.
In F13 the discussion of the effects of thermal inertia on the surface temperature was simplified, just describing the differences of results between the soil (surface albedo of ~0.22 in average and thermal inertia of 250 J $s^{-1/2}$ m^{-2} K^{-1}, hereafter the unit is omitted) and ice (surface albedo of 0.4 and thermal inertia of 1,000) surfaces. If ancient Martian surface was covered with wet and ice-free soil, the thermal inertia should become much larger than that of today, with the surface albedo of lower than 0.4 (the ground covered by ice). In this case, the results of surface temperature should be different from those which have been shown in F13.
From this point of view, we performed the simulations of the ancient Martian environment, especially focusing on the sensitivity of thermal inertia, using our improved MGCM, DRAMATIC (Dynamic, RAdiation, MAterial Transport and their mutual InteraCtions) [e.g., Kuroda et al., 2005]. We assumed the pure CO_2 atmosphere as F13. We have implemented the radiative effects of CO_2 gas assuming the sub-Lorentzian profile [Fukabori et al., 1986] and considering also the collision induced absorptions [Gruszka and Borysow, 1997]. For the comparison with F13’ s results, the obliquity, eccentricity, surface albedo and thermal inertia are set to be the same as their standard simulation. Also the vertical coordinate of the model is set to 15 layers to ~50 km altitude, as well as F13, and horizontal resolution is set to 64x32 (5.625deg latitude by 5.625deg longitude). The radiative effects of CO_2 ice clouds are also considered in solar and infrared wavelengths as well as F13, although the radiative effects of dust are not considered.
At first, in order to check the validity of our model, we simulated with globally constant thermal inertia of 250 (soil) for the globally averaged surface pressure of 0.1 –3 bars (realistic pressure range of early Mars). The results showed that annual mean surface temperature in the equilibrium state increased with surface pressure, but the annual mean temperature was ~225 K for 2 bars and ~237 K for 3 bars, far below the H_2O melting point. The infrared optical depth of CO_2 ice clouds reached the highest value of τ ~1.4 for the surface pressure of 1.5 bars, probably because of the profiles of CO_2 condensation temperature and simulated annual-mean temperature against surface pressure which indicated the most favorable production of CO_2 ice clouds at ~1.5 bars. The radiative effects of CO_2 ice clouds affect to increase the global mean temperature for several Kelvins in maximum, while ~10 K in F13.
Next, we simulated with globally constant thermal inertia of between 1,000 (ice) and 5,000 (wet soil assumption) for the surface pressure of 2 and 3 bars. The results showed that annual mean surface temperature in the equilibrium state greatly increased with increased thermal inertia. Daily mean surface temperatures in northern low- and mid-latitudes and Hellas basin, where are in low altitude and

considered to be the places of ancient ocean/lake, are above 273 K almost throughout the Martian year for 3 bars and thermal inertia of 5,000.
Our results suggest that the surface conditions could be the key of the existence of liquid water in early Mars. The surface with high thermal inertia may be able to produce the surface temperature higher enough to keep liquid water even with the pure CO_2 atmosphere under the solar insolation which was ~75% of today.

Keywords: Mars, paleoclimate, thermal inertia, GCM, sub-Lorentzian, collision induced absorption

Stratified hybrid-type proto-atmosphere on accreting Mars

*Hiroaki Saito[1], Kiyoshi Kuramoto[1]

1. Department of Cosmosciences, Graduate School of Sciences, Hokkaido University

The precise Hf-W chronology suggests that Mars reached about half of its present mass within the 1.8 ± 1.0 Myr or less after the formation of CAI with core-mantle differentiation (Dauphas and Pourmand, 2011). Since this timescale is much shorter than the estimated lifetime of the solar nebula, the accretion of Mars mostly proceeded within the solar nebula. On the other hand, the energy released by planetesimals collisions becomes large enough to induce degassing of the volatile compounds such as H_2O when the proto-Mars gets bigger than the lunar size (0.1 M_M). Therefore, growing Mars may have a proto-atmosphere that consists of nebula gas and degassed gas.

We analyze the thermal structure of stratified hybrid-type proto-atmosphere where the solar nebula component dominates the upper layer, and the degassed component dominates the lower layer, by developing a 1D radiative-equilibrium model. Provided that the building blocks of Mars are described by the two-component model, which contains 4 wt% of volatiles, a hot proto-atmosphere is formed with the surface temperature exceeding the melting point of rocks (1500K) when accretion time is within 4 Myr. This suggests that the core-mantle differentiation efficiently proceeds due to the formation of a magma ocean produced by the atmospheric blanketing effect.

However, there is a possibility that the proto-atmosphere may be mixed due to convection or molecular diffusion. The mixing of the proto-atmosphere possibly changes the thermal structure of the proto-atmosphere. There is also uncertainty for the volatile concentration in the building blocks.

In this study, we investigate condition for keeping atmospheric stratification by comparing the level of the compositional boundary (CB) and the tropopause, and the accretion time and mass exchange time scale controlled by molecular diffusion. The accretion times is taken from 1 –6 Myr as the chronology suggests. In the case of the volatile concentration is 4 wt%, we found that the level of the CB is always above the tropopause for any accretion times and proto-Mars mass, which means convective mixing between the solar nebula layer and degassed component layer does not occur. Moreover, the mass exchange time scale is about 10^2 times longer than the accretion time. Thus the mixing by molecular diffusion is unlikely to occur. On the other hand, when the volatile concentration is less than 2 wt%, the level of the tropopause is located above the level of the CB, and therefore the convective mixing occurs across the solar nebula layer and the degassed component layer. The resultant changes in the thermal structure of the proto-atmosphere are now under study.

Keywords: Proto Mars, Proto-Atmpsphere

Increase in ferrous ion by soaking basalt in acid water solution and UV rays

*Nobuo Komori[1]

1. Ota Ward Kamata Junior High School

Recent proven by the Mars explorer, it was shown that there was an ocean on Mars 43 billion years ago. That ocean might have been made of acid. Having this ocean as a precondition I did two following experiments to test this theory about mars.
In the first experiment, I measured density of ferrous ion which went into two kinds of solution ;solution neutralizing sulfuric and basalt: hydrochloric acid and basalt.
My result was that about 5 times more ferrous ion dissolved in pH1 hydrochloric acid than in pH2. In the second experiment I measured the density of ferrous ion in the case of going into solution when fayalite and basalt were soaked in purified water, hydrochloric acid, and sulfuric. And the other case was in the same condition with UV irradiated. Results show the denstiy of ferrous ion in the case of UV irradiation was 1.5 times higher than non UV irradiation.
As a result of these experimental results, a large quantity of ferrous ion might have been dissolved in Mar’ s ocean because of the neutralization of the acid by rocks such as basalt. Furthermore, dissolved ferrous ion might have been increased by solar ultraviolet rays C.

Keywords: ultraviolet rays, ferrous ion, fayalite, basalt, acid aqueous solution

Origin of Solar system is explored by the question "Why?". Operation of Planet was elucidated by Newton's law. “Multi-impact hypothesis” that unifiedly explains Origins of Asteroid belt, Moon, Jupiter's red spot, using Abduction.

*Akira Taneko[1]

1. SEED SCIENCE Lab.

Proof by abduction (a means of exploring the origin to the past where neither the earth nor human beings are formed), if it can explain the current multiple mystery in a unified manner with a hypothesis having a physical meaning, the evolution and history of Yuichi's solar system I understand that the validity of the hypothesis was supported as the truth verified by.The hypothesis which can show the basis of the origin is groundbreaking as an effective means of the origin problem of geophysics which can neither experiment nor theoretically calculate.

In Multi-Impact Hypothesis, *CERRA is formed at Cerres position in Bode's rule, the eccentricity increases by Jupiter perturbation.* **Sera split about 4 billion years ago by Jupiter's tidal power and became Origin of Aasteroid belt.**
Furthermore, Mantle fragments crashed into Earth (12.4 km / s, 36.5 degrees: value derived from Hypothesis) and Moon was formed at Current distance (60RE). Collision position was Pacific Ocean and Crust peeling trace was Isostasy and became Darwin uplift. Multi-Impact of Multiple iProof by abduction (a means of exploring the origin to the past where neither the earth nor human beings are formed), if it can explain the current multiple mystery in a unified manner with a hypothesis having a physical meaning, the evolution and history of Yuichi's solar system I understand that the validity of the hypothesis was supported as the truth verified by.mpact is Origin of extinction of species, cause Mantle cracks and Formation of plate boundary, It is also Origin of deep ocean floor and Earth twin frequency formation. Earth rotation and Earth core eccentricity and effect of inertial efficiency unbalance compensation were shown as driving force of plate tectonics, Wegener's continental drift theory and ocean floor update theory etc.
Furthermore, Origins of Pacific arcuate archipelago and back arc basin, Mantle exfoliation and Isostasy due to collision, Pressing of Concave plate basin and Convex plate are Origins of mutual slip between Origins of Average depth of 5 km.
Driving force of plate tectonics is due to Inertial efficiency of Earth due to imbalance due to Mantle collision peeling and equalization due to Direction of rotation of Earth. Plate boundary is Mantle crack at Time of collision, Melting point drops due to Pressure decrease and Mantle melts.

Keywords: Elucidation of origin by abduction, actial proof by one-time evolution, Proof of Titius Bode's Law, Mechanism of Accumulation, Origin of the moon, Origin of asteroid belt and meteorite, Origin of Jupiter Large Red Spot, Origins of deep ocean floor

The Origin of The Moon and The deep sea floor bottom and Plate-Tectonics elucidated with Multi-Impact Hypothesis.

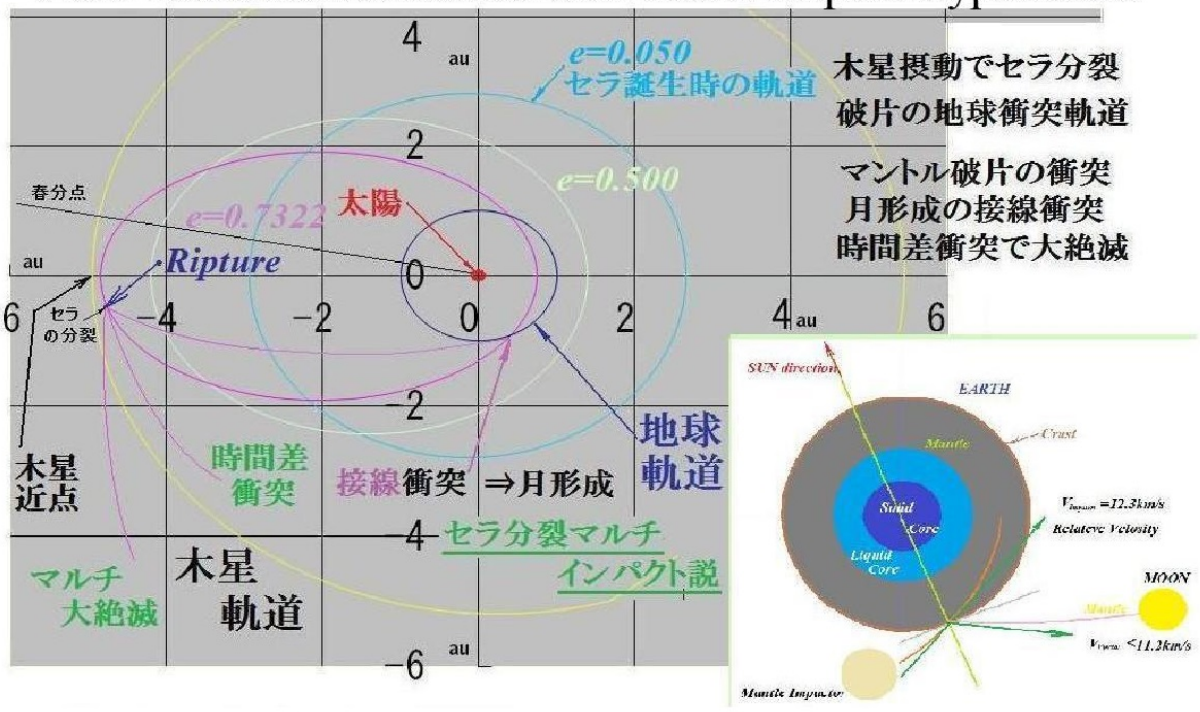

O8-08 The Origin of the Deep Ocean Floor and the Plate-Tectonics, Elucidation of the Driving Force, The Origin of the Moon and the Earth Deep Ocean Floor with Multi-Impact Hypothesis *2016 9-14*

8. プレートの駆動力,同じ密度のプレートが上下に重なる理由

8.1. プレートの駆動力は謎であった. ①.マントル対流仮説(.ホームズ)
②.前引き,後押し仮説 ③.リソスフェア厚さ傾斜仮説 ④.プリューム仮説
⑤. 慣性モーメントアンバランス解消偶力説 (本仮説) 偏芯の解消偶力.
マルチインパクト仮説で地殻プレートが図Aの状態⇒図Bの均質安定状態.

8.2. 同じ密度のプレートが他方の下に潜り込んで,海溝と和達・ベニオフ帯を形成するメカニズムの謎も有った. 衝突剥離時のアイソスタシーで凹海盆 α.

が形成された.
凸プレートと,凹プレートが押し合うと,凸プレートが折れ曲がって,凹プレートの下に潜り込む. β.
更に深く和達・ベニオフ帯を形成して,地震発生面に成る.